N94-18370

DC and Small-Signal Physical Models for the AlGaAs/GaAs High Electron Mobility Transistor

J. C. Sarker and J. E. Purviance
NASA Space Engineering Research Center for VLSI System Design
Department of Electrical Engineering
University of Idaho, Moscow, ID 83843

Abstract- **Analytical and numerical models are developed for the microwave small-signal performance, such as transconductance, gate-to-source capacitance, current gain cut-off frequency and the optimum cut-off frequency of the AlGaAs/GaAs High Electron Mobility Transistor (HEMT), in both normal and compressed transconductance regions. The validated I-V characteristics and the small-signal performances of four HEMTs are presented.**

Nomenclature

L : Gate length.
Z : Gate width.
μ_1 : Low field mobility of AlGaAs layer.
μ_2 : Low field mobility of two-dimensional electron gas.
d : Thickness of AlGaAs layer.
d_i : Thickness of undoped AlGaAs layer.
w : Width of undepleted region in AlGaAs layer.
N_d : Doping concentration of AlGaAs layer.
n_s : Sheet concentration of two-dimensional electron gas.
n_{so} : Equilibrium Sheet concentration of two-dimensional electron gas.
ϵ_2 : Permittivity of AlGaAs.
E_{c1} : Saturation electric field of AlGaAs.
E_{c2} : Saturation electric field of two-dimensional electron gas.
v_s : Saturation velocity of two-dimensional electron gas.
β : Charge control coefficient.
δ : Effective width of conduction channel.
V_{tho} : Threshold voltage for two-dimensional electron gas.
V_{bi} : Built-in voltage of Schottky gate on AlGaAs layer.
V_p : Effective pinch-off voltage of AlGaAs layer.

1 Introduction

High frequency solid state technology has been moving towards the use of the high electron mobility transistors in microwave and in high speed digital circuits because of its high frequency operation and of its tolerance to many forms of radiation. Several workers have been studying the GaAs HEMTs both theoretically and experimentally since its first introduction in 1980 [1]. Over the past years, analytical, numerical and/or computer-aided

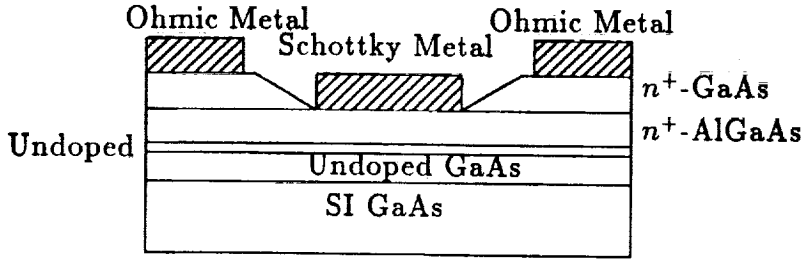

Figure 1: Schematic Diagram of a Uniformly Doped AlGaAs/GaAs HEMT.

models have been reported by many authors. But, because of the complexity in structure of this device, VLSI circuit designers demand a more accurate and compact model for their design.

Among other workers, C.Z. Cil and S. Tansal [2], in 1985, proposed an analytical model which used the simple Trofimenkoff-type velocity-field linear relation [3]. Their modeled results agree very well with the experimental data. However, their model is good only for the linear normal transconductance region; it does not cover the current saturation region and also the parasitic conduction in the AlGaAs layer. But the computer-aided design and simulation of the HEMT circuits demand a complete and more accurate model. In 1986, G.W. Wang and W.H. Ku [4] developed a compact but complete analytical model which covers the whole operation range of the dc characteristics. This model calculates the I-V characteristics of four different HEMTs and compares the modeled results with the experimental data. We have chosen their model as the basis for this work and from this model we have developed analytical and numerical models to calculate the small-signal performances, such as transconductance, g_m, gate-to-source capacitance, C_{gs}, current gain cut-off frequency, f_T, and the optimum value of the cut-off frequency, $f_T(opt)$ before current saturation occurs.

2 DC Model

The basic structure of a HEMT device is significantly different from a conventional field effect transistor. A cross sectional view of a uniformly doped AlGaAs/GaAs HEMT device is shown in Figure 1.

At low gate voltage, it has only one current conduction channel but at high gate voltage, it has two conduction channels: one is the two-dimensional electron gas (2-DEG) in the interface between AlGaAs and GaAs and the other is the parasitic conduction through the undepleted n^+-AlGaAs layer. If the AlGaAs layer is not fully depleted by the Schottky gate and the heterojunction, then the free carriers under the gate are the two-dimensional electrons and the free electrons in the AlGaAs layer. The width of the undepleted AlGaAs

region can be approximated by [5]

$$w \approx d - d_i - \frac{n_{so}}{N_d} - \sqrt{\frac{2\epsilon_2}{qN_d}(V_{bi} - V_G)} \tag{1}$$

By setting $w = 0$, the AlGaAs layer is completely depleted, one can obtain the critical value of the gate voltage, V_G as

$$V_c = V_G(w = 0) = V_{bi} - \frac{qN_d}{2\epsilon_2}(d - d_i - \frac{n_{so}}{N_d})^2 \tag{2}$$

The $V_G \leq V_c$ defines the *normal transconductance region* where only the 2-DEG is the current conduction channel and the $V_G > V_c$ defines the *compressed transconductance region* where both the 2-DEG and the undepleted AlGaAs layer are the current conduction channels.

According to the charge control model [6], the sheet charge density of the 2-DEG can be approximated as a linear function of gate voltage and channel voltage which is given by

$$n_s(x) = \beta(V_G - V(x) - V_{th}) \tag{3}$$

where x is in the direction along the heterojunction.

In this dc model, for mathematical simplicity, the Trofimenkoff-type [3] electron velocity-field relation has been used for both the 2-DEG channel and the AlGaAs parasitic conduction channel. The linear electron velocity-field can be related as

$$v(x) = \frac{\mu E(x)}{1 + \frac{E(x)}{E_c}} \tag{4}$$

Here, $E(x)$ is the electric field in the 2-DEG channel or in the undepleted AlGaAs layer and E_c is the field at which the velocity of electrons reach the maximum value (saturation velocity).

Using the charge control concept and the velocity-field relationship described above, the current conducting through the 2-DEG channel can be determined by

$$I_{2-DEG} = Zqn_s(x)v(x) \tag{5}$$

Similarly, the current through the undepleted AlGaAs layer can be determined by

$$I_{AlGaAs} = ZqN_dw(x)v(x) \tag{6}$$

Here, for simplicity, full ionization of the donor atoms has been assumed for the current through the AlGaAs layer.

(A) I-V Equations in the Normal Transconductance Region

When the gate voltage is low, i.e. $V_G \leq V_c$, the normal transconductance region is formed. This region is then divided into the *linear* ($V_D < V_{sat}$) and the *saturation* ($V_D \geq V_{sat}$) regions. The current-voltage relationship in two different regions can be derived as follows:

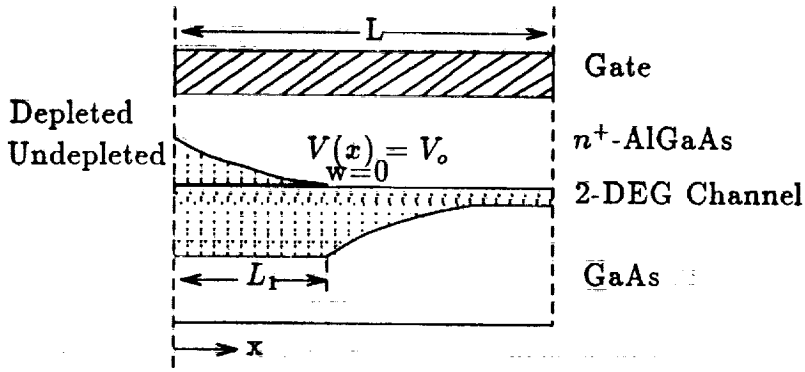

Figure 2: Schematic Diagram Showing Current Saturation in the 2-DEG Channel.

(i) Normal Linear Region ($V_D < V_{sat}$)
Introducing equations (3) and (4) in equation (5), and integrating from source to drain along the 2-DEG channel, the current through the channel is

$$I_D = \frac{A(V_G - V_{th} - \frac{V_D}{2})V_D}{1 + \frac{V_D}{B}} \tag{7}$$

where $A = \frac{Z q \beta \mu_2}{L}$ and $B = L E_{c2}$ are the model parameters; V_G and V_D are the internal gate and drain voltages.

(ii) Normal Saturation Region ($V_D \geq V_{sat}$)
The velocity-field relation (equation (4)) allows the velocity to saturate when the electric field approaches infinity. But physically it is impossible; so, the model assumed that the velocity saturation occurs when $E \geq E_c$. Therefore, from equation (4), the saturation velocity at $E = E_c$ is $v_s = \frac{\mu E_c}{2}$.

When the drain voltage, V_D becomes greater than the saturation voltage, V_{sat} the situation becomes like Figure 2. At $x = L_c$, electric field exceeds saturation field, E_c, and the electron velocity saturates; and after this the electrons move with this constant saturation velocity. Then, using $V = V_{sat}$ and $\frac{dV}{dx} = E_{c2}$ at $x = L_c$, equation (7) can be written as

$$I_D = \frac{Z q \beta \mu_2 (V_G - V_{th} - \frac{V_{sat}}{2})V_{sat}}{L_c + \frac{V_{sat}}{E_{c2}}} \tag{8}$$

Also from equations (3) and (5), the current in the saturation region can be written as

$$I_D = Z q \beta (V_G - V_{th} - V_{sat}) v_s = \frac{Z q \beta \mu_2}{2} (V_G - V_{th} - V_{sat}) E_{c2} \tag{9}$$

Now, using the current continuity condition, equations (8) and (9) can be combined to obtain

$$V_{sat} = \frac{(1 - K_1)B(V_G - V_{th})}{(1 - K_1)B + (V_G - V_{th})} \tag{10}$$

where $K_1 = \frac{L-L_c}{L}$. Generally, L_c and V_{sat} can be determined by solving a two-dimensional Poisson's equation which has the form in the velocity saturation region

$$\frac{\partial^2 V}{\partial x^2} \approx \alpha I_D \tag{11}$$

where $\alpha = \frac{1}{\epsilon_2 v_s Z \delta}$. Here, δ is the effective width of the conduction channel which is assumed to be invariant to the bias voltage as compared to I_D and set to a constant. This Poisson's equation is obtained by neglecting the variation of carrier concentration in the direction perpendicular to the channel and can be solved with boundary conditions $V(L = L_c) = V_{sat}$ and $E(L = L_c) = E_c$. The final form of the solution becomes

$$V_D - V_{sat} = \frac{\alpha I_D (L - L_c)^2}{2} + E_{c2}(L - L_c) = C I_D K_1^2 + B K_1 \tag{12}$$

where $C = \frac{\alpha L^2}{2} = \frac{L^2}{2\epsilon_2 Z v_s \delta}$ is the third model parameter. Equations (10) and (12) can be solved simultaneously to find K_1 and V_{sat} :

$$K_1 = \frac{-X + \sqrt{X^2 + [2CA(V_G - V_{th})^2 - 4B][1 + \frac{(V_G - V_{th})}{B}]V_D}}{CA(V_G - V_{th})^2 - 2B} \tag{13}$$

where $X = B + V_D + V_G - V_{th}$. Then from equation (8), the saturation current equation can be written as

$$I_D = \frac{A(V_G - V_{th} - \frac{V_{sat}}{2})V_{sat}}{1 - K_1 + \frac{V_{sat}}{B}} \tag{14}$$

(B) I-V Equations in the Compressed Transconductance Region

When the gate voltage is high enough such that $V_G > V_c$, the AlGaAs layer starts to conduct current. This current conduction mechanism can be considered similar to a parasitic MESFET and it is shown in Figure 3.

When $w = 0$ at $x = L_1$, from equation (1) the voltage inside the channel is $V = V_o = V_p - V_{bi} + V_G$, where V_p is defined as

$$V_p = \frac{qN_d}{2\epsilon_2}(d - d_i - \frac{n_{so}}{N_d})^2 \tag{15}$$

When $V_D \leq V_o$, the sheet carrier concentration, n_s of the whole 2-DEG channel is equal to its equilibrium value, n_{so} and it is independent of gate and drain voltage. The 2-DEG channel is then like a non-linear resistor with sheet concentration, n_{so}, while the undepleted AlGaAs behaves like a MESFET. This equilibrium concentration is assumed to be maximum and is given by (from equation (3))

$$n_{so} = \beta(V_{bi} - V_p - V_{th}) \tag{16}$$

¿From the schematic diagram shown in Figure 3, the compressed transconductance region can be divided into three different regions of operation :

(i) Linear Region I : $V_D \leq V_o$

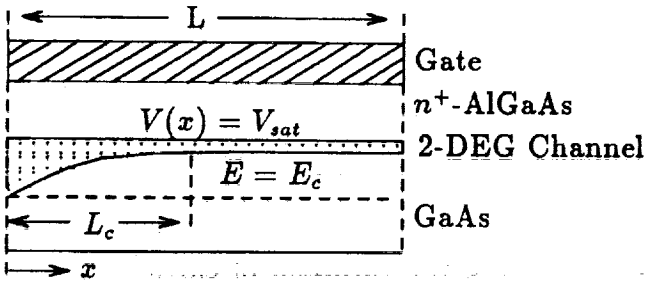

Figure 3: Schematic Diagram Showing Current Saturation in the 2-DEG Channel and the Parasitic Conduction through the AlGaAs Layer.

(ii) Linear Region II : $V_o < V_D < V_{sat}$
(iii) Saturation Region : $V_D \geq V_{sat}$
Here, the assumption $V_{sat} \geq V_o$ has been made to allow division into various regions of operation. This assumption is true for typical HEMT devices.
(i) Linear Region I
For $V_D \leq V_o$, the current through the AlGaAs layer is derived as in the case of the MESFET and is given by

$$I_1 = \frac{E}{1 + \frac{V_D}{F}} \left[V_D - \frac{2}{3} \frac{(V_{bi} - V_G + V_D)^{3/2} - (V_{bi} - V_G)^{3/2}}{\sqrt{V_p}} \right] \tag{17}$$

where $E = \frac{Zq\mu_1 N_d}{L}(d - d_i - \frac{n_{so}}{N_d})$ and $F = LE_{c1}$ are two more model parameters.
The current through the 2-DEG channel becomes

$$I_2 = \frac{A(V_{bi} - V_p - V_{th})V_D}{1 + \frac{V_D}{B}} \tag{18}$$

The total current in this region of operation is the sum of these two currents : $I_D = I_1 + I_2$.

(ii) Linear Region II
¿From Figure 3, for $V_D > V_o$, the current flowing through the 2-DEG channel is

$$I_2 = \frac{Zq\mu_2 n_{so} V_o}{L_1 + \frac{V_o}{E_{c2}}} \tag{19}$$

¿From this equation

$$L_1 = \frac{Zq\mu_2 n_{so} V_o}{I_2} - \frac{V_o}{E_{c2}} \tag{20}$$

Current through the AlGaAs layer can be obtained from equation (6) as

$$I_1 = \frac{Zq\mu_1 N_d w \frac{dV}{dx}}{1 + \frac{1}{E_{c1}} \frac{dV}{dx}}$$

Integrating this equation for V from 0 to V_o and for x from 0 to L_1, and then using equation (20) for L_1, the final expression for current becomes

$$I_1 = \frac{E\left[V_o - \frac{2}{3}(V_p - \frac{(V_{bi}-V_G)^{3/2}}{\sqrt{V_p}})\right]}{\left[\frac{A(V_{bi}-V_p-V_{th})}{I_2} - \frac{1}{B} + \frac{1}{F}\right]V_o} \tag{21}$$

The derivation of the current expression in the 2-DEG is similar to the normal region. But here, the limits of integration for V are from V_o to V_D and for x from L_1 to L. After performing the integration and using equation (20) for L_1, the current through the 2-DEG channel can be obtained as

$$I_2 = \frac{A[(V_G - V_{th} - \frac{V_D+V_o}{2})(V_D - V_o) + (V_{bi} - V_p - V_{th})V_o]}{1 + \frac{V_D}{B}} \tag{22}$$

So, the total drain current is the sum of equations (21) and (22).

(iii) Saturation Region

For the saturation region, $V_D \geq V_{sat}$, the current expression for the undepleted AlGaAs layer is the same as the linear region II (equation (21)). The principle to find the saturation voltage in this operating region is similar to that in the normal region except the contribution from the parasitic conduction has to be taken into account. From the current continuity at the interface of the velocity saturation region and the non-saturation region (Figure 3), the saturation voltage can be obtained as

$$V_{sat} = \frac{[(1 - K_1)B(V_G - V_{th}) + 2(V_G - V_{bi} + V_p)V_o - V_o^2]}{[(V_G - V_{th}) + (1 - K_1)B]} \tag{23}$$

On the other hand, the solution of the Poisson's equation (equation (12)) in this region becomes

$$V_D - V_{sat} = \frac{CAK_1^2\left[(V_G - V_{th})V_{sat} - \frac{V_{sat}^2}{2} - (V_G - V_{bi} + V_p)V_o + \frac{V_o^2}{2}\right]}{1 - K_1 + \frac{V_{sat}}{B}} + BK_1 \tag{24}$$

By solving equations (23) and (24) iteratively, values of K_1 and V_{sat} can be found. Once K_1 and V_{sat} are found, the current through the 2-DEG channel can be obtained as

$$I_2 = \frac{A[(V_G - V_{th} - \frac{V_{sat}+V_o}{2})(V_{sat} - V_o) + (V_{bi} - V_p - V_{th})V_o]}{1 - K_1 + \frac{V_{sat}}{B}} \tag{25}$$

The total drain current is then the sum of equations (21) and (25).

In the subthreshold region of operation the charge control is not linear; so, in addition to the model and physical parameters, a fitting parameter, D is used to model the threshold voltage shift of the 2-DEG caused by the drain voltage. This simple threshold voltage correction is given by

$$V_{th} = V_{tho} - D \times V_D \tag{26}$$

So, with the nine parameters A, B, C, E, F, V_p, V_{tho}, V_{bi} and D, the I-V characteristics of the AlGaAs/GaAs HEMT device can be modeled completely.

3 Small-Signal Model

Evaluation and analysis of the small-signal performances of the HEMT are important for the operation of microwave circuits. The HEMT is usually biased in the normal transconductance region without parasitic conduction for optimal low-noise and/or high-frequency performance. Some of the small-signal parameters like transconductance, gate-to-source capacitance, current gain cut-off frequency etc. can be derived analytically from this model. The derivation of these parameters in the saturated normal region and also in the compressed transconductance region is mathematically complicated and computationally involves more CPU time. So, to determine these parameters in those regions of operation a computationally efficient numerical technique has been used. Methods of determining of these small-signal parameters are discussed in the next few subsections.

3.1 Transconductance, g_m

The intrinsic transconductance, g_m at constant drain voltage is defined as

$$g_m \equiv \frac{\partial I_D}{\partial V_G} \mid_{V_D=Constant}$$

The g_m in the linear normal region can be obtained analytically by differentiating drain current (equation (7)) with respect to gate voltage :

$$g_m = \frac{\partial}{\partial V_G}\left[\frac{A(V_G - V_{th} - \frac{V_D}{2})V_D}{1+\frac{V_D}{B}}\right] = \frac{AV_D}{1+\frac{V_D}{B}} \tag{27}$$

The transconductance increases with drain voltage before current saturation and is inversely proportional to gate length and mobility degradation factor $(1 + \frac{V_D}{B})$.

To calculate g_m in the saturation region and in the compressed (both linear and saturation) region, we differentiate the corresponding drain currents numerically. For this numerical differentiation we have used the centered-finite-divided difference equation of the form [7]

$$g_m(V_{G_i}) = \frac{I_D(V_{G_{i+1}}) - I_D(V_{G_{i-1}})}{V_{G_{i+1}} - V_{G_{i-1}}} \tag{28}$$

Here, $g_m(V_{G_i})$ is the transconductance evaluated at the i^{th} point.

3.2 Gate-to-Source Capacitance, C_{gs}

Gate-to-source capacitance, C_{gs} is defined, with the assumption $C_{gd} \ll C_{gs}$, as

$$C_{gs} \equiv \frac{\partial Q_T}{\partial V_G}$$

where Q_T is the total charge.

In the normal region, the AlGaAs layer is completely depleted, so the C_{gs} is due only to the two-dimensional electron gas. Thus, for the normal region

$$C_{gs} = \frac{\partial}{\partial V_G}\left[\int_0^L q n_s(x) dx\right]$$

Substituting equation (3) for $n_s(x)$ and then performing the integration, we get

$$C_{gs} = \frac{\partial}{\partial V_G}\left[\int_0^L q\beta(V_G - V(x) - V_{th})dx\right] = \frac{AL^2(2+\frac{V_D}{B})}{\mu_2} \tag{29}$$

Calculation of gate-to-source capacitance in the saturation region is more complicated because of complexity in the total charge calculation in the channel. The method we have used to calculate the charge in the channel is given in detail in reference [8]. The final expression of total charge, Q_T becomes

$$Q_T = \frac{AL}{\mu_2}\left[(V_G - V_{th})L - V_{sat}(L - \frac{L_c}{2})\right] \tag{30}$$

where

$$L_c = -\frac{V_{sat}L}{B} + \frac{AL(V_G - V_{th} - \frac{V_{sat}}{2})V_{sat}}{I_D} \tag{31}$$

In this equation, the saturation current, I_D is calculated by using equation (14) at the saturation voltage, V_{sat}.

Once we know the total charge in the channel we can calculate the C_{gs} by using numerical differentiation. The form of this differentiation is analogous to the g_m equation

$$C_{gs}(V_{G_i}) = \frac{Q_T(V_{G_{i+1}}) - Q_T(V_{G_{i-1}})}{V_{G_{i+1}} - V_{G_{i-1}}} \tag{32}$$

Ideally, to calculate C_{gs} in the compressed region, the capacitance due to the charge accumulated in the undepleted AlGaAs layer has to be added with the capacitance due to the 2-DEG channel. But the calculation of the capacitance due to AlGaAs layer analytically from this model is not very straightforward. Moreover, this additional capacitance contribution may not be very significant, particularly at high drain voltages. So, in this work we have neglected this contribution compared to the capacitance due to the 2-DEG channel charge. Therefore, equation (32) has also been used to calculate the gate-to-source capacitances in the compressed transconductance region.

3.3 Current Gain Cut-off Frequency, f_T

In microwave applications, the current gain cut-off frequency is the frequency used as an indicator of the device speed. The conventional definition of f_T is

$$f_T \equiv \frac{g_m}{2\pi C_{gs}}$$

In the normal linear region, we calculated f_T analytically by using equations (27) and (29):

$$f_T = \frac{1}{2\pi}\left[\frac{AV_D}{1+\frac{V_D}{B}}\right]\left[\frac{\mu_2}{AL^2(2+\frac{V_D}{B})}\right] = \frac{\mu_2 V_D}{2\pi L^2(1+\frac{V_D}{B})(2+\frac{V_D}{B})} \tag{33}$$

We again adopted the numerical techniques to calculate f_T for normal saturated region and both linear and saturated compressed regions. This numerical expression is given by

$$f_T(V_{G_i}) = \frac{g_m(V_{G_i})}{2\pi C_{gs}(V_{G_i})} \tag{34}$$

Here, the f_T, g_m and C_{gs} are calculated at the i^{th} point.

3.4 Optimum Cut-off Frequency, f_T(opt)

Another important parameter in microwave applications is the optimum frequency, f_T(opt). This optimum frequency is defined as the maximum value of the current gain cut-off frequency just before current saturation occurs. Thus, in the normal transconductance region, f_T(opt) is approximated as

$$f_T(opt) = \frac{\mu_2 V_{sat}}{2\pi L^2(1+\frac{V_{sat}}{B})(2+\frac{V_{sat}}{B})} \tag{35}$$

Here, V_{sat}, the value of the saturation voltage when current just starts to saturate, can be evaluated by setting $K_1 = 0$ in equation (10) :

$$V_{sat} = \frac{B(V_G - V_{th})}{B + (V_G - V_{th})} \tag{36}$$

4 Results and Discussion

4.1 The I-V Characteristics

To validate the dc model we have developed a computer simulation program which calculates the I-V characteristics over the entire region of operation. Using this simulation program we have calculated the I-V characteristics of all the four HEMTs. The device physical parameters and the modeling parameters of these HEMTs, taken from reference [4], are given in Table 1.

In the derivation of the drain current equations in section 2, the dc model does not include the effects of parasitic source and drain resistances explicitly. These effects can be taken into account in the model by solving the nonlinear equations which are given below

$$V_{GS} = V_G + I_D(V_G, V_D)R_S \tag{37}$$

and

$$V_{DS} = V_D + I_D(V_G, V_D)(R_S + R_D) \tag{38}$$

Device	HEMT #1 (TRW #2078)	HEMT #2	HEMT #3 (GE #5410)	HEMT #4
L(μm)	0.35	1.0	0.25	1.0
Z(μm)	65	145	100	1200
$V_{tho}(V)$	-0.017	-0.901	-0.912	-2.389
$V_p(V)$	-	-	1.481	2.319
$V_{bi}(V)$	-	-	0.85	0.85
$A(mA/V^2)$	49.517	101.253	103.539	454.167
B(V)	5.285	1.604	0.616	0.948
$C(K\Omega)$	8.341	0.583	0.992	0.201
D	0.015	0	0.092	0.008
E(mA/V)	-	-	81.825	542.663
F(V)	-	-	2.154	3.04
$R_S(\Omega)$	5.9	7.0	4.6	1.0
$R_D(\Omega)$	6.0	7.0	6.0	1.0

Table 1: Physical and Model Parameters of the HEMTs.

where V_{GS} and V_{DS} are the externally applied gate and drain voltages respectively; R_S and R_D are the parasitic source and drain resistances. These two equations were solved iteratively in the program to find the values of V_G and V_D for given values of external voltages V_{GS} and V_{DS}.

The HEMT #1 and #2 show only normal transconductance effects; only five model parameters, V_{tho}, A, B, C and D are needed in the program to calculate the I-V relation. With these parameter values and using equations (7), (10), (13), (14), (37) and (38), we have developed a simulation program which calculates the drain-to-source current as a function of external drain voltage for different external gate voltages.

Figure 4 shows the I-V curve of the HEMT #1. In the program, we have swept the drain voltage from 0 to 3 volts with a 0.2 volts steps and calculated drain-to-source currents for gate voltages V_{GS} = 0, 0.1, 0.2, 0.3, 0.4 and 0.5 volts. As a comparison, we have also plotted the experimental data obtained from reference [4]. From the figure, we can see a nice agreement between our I-V results and the experimental data.

Simulated results along with experimental data [4,6] of the HEMT #2 are shown in Figure 5. In this case the drain voltage was varied from 0 to 3 volts with 0.25 volts steps. Drain currents for V_{GS} = -0.8, -0.6, -0.4, -0.2 and 0 volts were calculated. The low gate bias curves agree very well with the experimental values. As the gate bias increases a small deviation occurs near the linear and saturation transition region.

The I-V characteristics of the HEMT #3 and #4 (double heterojunction HEMT) are more complex because of the compressed transconductance effect (in addition to the normal transconductance effect). Four additional parameters V_p, V_{bi}, E and F are needed to model this effect. So, with the nine parameter values listed in Table 1 and using the equations (17), (18) and (21-25), we have calculated the drain-to-source currents in the compressed transconductance region. Equation (24) was rearranged such that K_1 can be written in

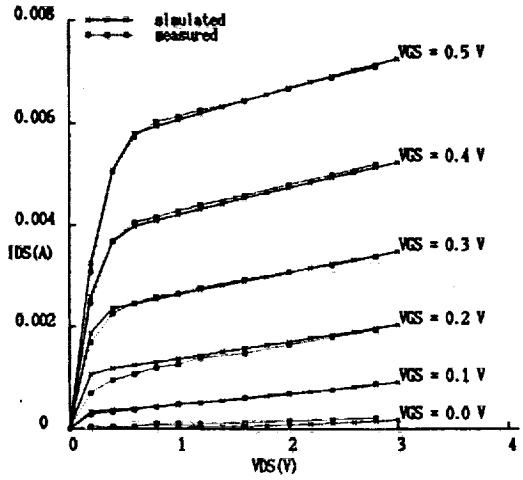

Figure 4: Characteristics of HEMT #1

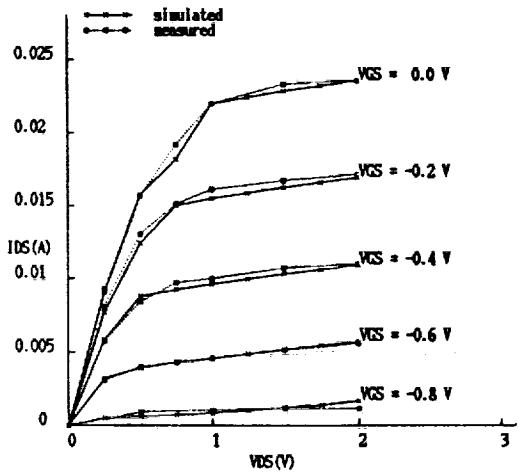

Figure 5: I-V Characteristics of HEMT #2

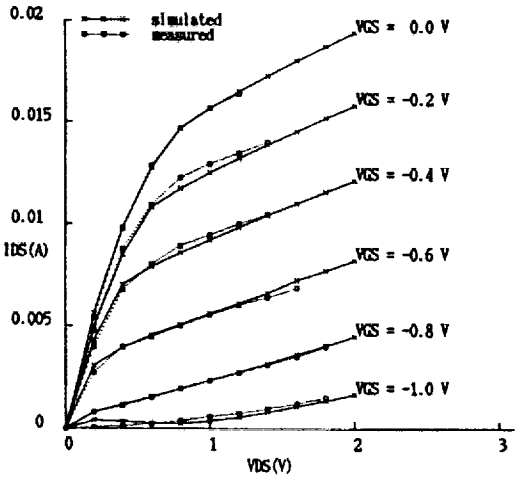

Figure 6: Characteristics of HEMT #3

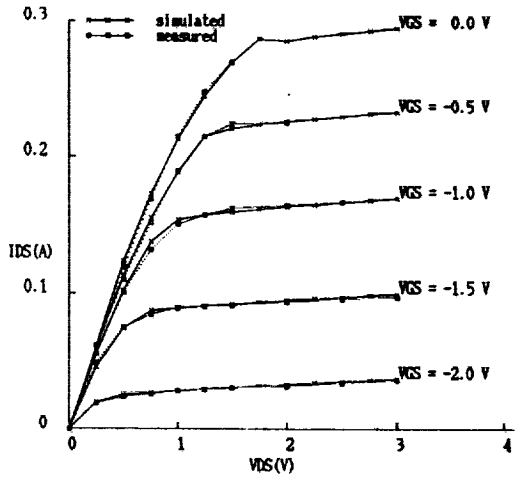

Figure 7: I-V Characteristics of HEMT #4

Device	Bias Condition	$I_D(mA)$	$g_m(mS)$	$C_{g_s}(fF)$	$f_T(GHz)$	$f_T(opt)(GHz)$
HEMT #1	Normal Linear Region $V_{GS} = 0.4V$, $V_{DS} = 0.4V$	3.677	16.526	28.501	92.283	96.055
HEMT #1	Normal Saturation Region $V_{GS} = 0.2V$, $V_{DS} = 1.0V$	1.376	10.868	6.5129	265.58	-
HEMT #2	Normal Linear Region $V_{GS} = -0.2V$, $V_{DS} = 0.5V$	12.389	27.471	507.09	8.622	10.698
HEMT #2	Normal Saturation Region $V_{GS} = -0.2V$, $V_{DS} = 1.0V$	15.461	31.098	134.89	36.692	-
HEMT #3	Normal Linear Region $V_{GS} = -0.65V$, $V_{DS} = 0.2V$	2.517	14.005	33.553	66.432	69.527
HEMT #3	Normal Saturation Region $V_{GS} = -0.8V$, $V_{DS} = 1.0V$	2.395	14.513	9.441	244.66	-
HEMT #3	Compressed Linear Region $V_{GS} = -0.2V$, $V_{DS} = 0.4V$	8.476	6.699	27.512	38.750	-
HEMT #3	Compressed Saturation Region $V_{GS} = -0.4V$, $V_{DS} = 1.0V$	9.215	16.924	11.344	237.45	-
HEMT #4	Normal Linear Region $V_{GS} = -1.5V$, $V_{DS} = 0.5V$	74.628	116.277	1583.0	11.89	13.18
HEMT #4	Normal Saturation Region $V_{GS} = -1.5V$, $V_{DS} = 1.0V$	88.939	133.306	500.9	42.36	-
HEMT #4	Compressed Linear Region $V_{GS} = -0.5V$, $V_{DS} = 1.0V$	188.287	48.913	1113.0	6.996	-
HEMT #4	Compressed Saturation Region $V_{GS} = -1.0V$, $V_{DS} = 1.0V$	153.567	123.322	548.7	35.77	-

Table 2: Small-Signal Performances of the AlGaAs/GaAs HEMTs Calculated in this Work.

curves for four HEMTs were successfully calculated and compared with the experimental data reported earlier [4,6].

In the second phase of the work, analytical and numerical methods were developed to predict some of the important small-signal performances of these HEMTs. Based on this new computer-aided model, the small-signal parameters, g_m, C_{g_s}, f_T and $f_T(opt)$ were calculated and are presented in Table 2. The proposed small-signal model for the AlGaAs/GaAs HEMT device may be useful to VLSI and microwave applications in future.

6 Acknowledgment

The authors acknowledge NASA for funding this project under the grant NAG5-1043. They would like to thank the NASA Space Engineering Research Center, University of Idaho for partial funding and for providing facilities to accomplish this work. The second author acknowledges Jesus of Nazareth for His sacrifice and example.

terms of V_{sat}

$$K_1 = \frac{-(B+V_D)+\sqrt{(B+V_D)^2+4[CAY-B][(1+\frac{V_{sat}}{B})(V_D-V_{sat})]}}{2\{CAY-B\}} \tag{39}$$

where $Y = (V_G - V_{th})V_{sat} - \frac{V_{sat}^2}{2} - \frac{V_G^2}{2}$. Equations (23) and (39) were solved iteratively in the program by assuming an initial value of $K_1 = 0$ to obtain V_{sat} and then K_1. After K_1 and V_{sat} are known, the drain current through the 2-DEG channel in the saturation region is calculated by using equation (25).

Figure 6 shows the I-V curve of the HEMT #3. Here, we have scanned the drain voltage from 0 to 3 volts at a step of 0.2 volts for the gate voltages, V_{GS} = -1.0, -0.8, -0.6, -0.4, -0.2 and 0 volts. As we can see the modeled result agrees very well with the experimental data [4].

Finally, we have calculated the I-V characteristics of a double heterojunction HEMT (HEMT #4) and the results, along with the experimental data are shown in Figure 7. These results also agree fairly well with the published measured data [4].

Two of the four HEMTs (HEMT #1 and #3) are sub-half-micron gate HEMTs. Unmodeled short channel effects such as velocity overshoot and unmodeled hot carrier effects may occur in these two HEMTs. It is reported that these effects start to become prominent below $0.25\mu m$ gate length [9], therefore HEMT #3 may show considerable short channel effect in the compressed transconductance region. Moreover, this dc model was originally developed only for the single-heterojunction HEMT. But from our simulation results of HEMT #4, which is a double-heterojunction HEMT, we found that this model also appears to be good for the double-heterojunction HEMT.

4.2 Small-Signal Performance Calculation

Based on the equations derived in section 3 and the physical parameters listed in Table 1, we have developed the simulation program which calculates the small-signal performances. Using this program we have calculated I_D, g_m, C_{gs}, f_T and f_T(opt) as a function of gate voltage keeping drain voltage fixed. Table 2 shows the small-signal parameter values for all the four HEMTs for different drain and gate bias conditions.

This small-signal model has been developed in an academic environment, based on a quasi-static approximation. The values of the small-signal parameters are essentially theoretical and have not been rigorously validated in this work because of the unavailability of the experimental data.

5 Conclusion

A complete analytical dc model for the uniformly doped AlGaAs/GaAs HEMT device has extensively analyzed and validated independently. Based on the model a simulation program was developed to calculate the I-V characteristics. Using this program, the I-V

References

[1] T. Mimura, S. Hiyamiza, T. Fujii, and K. Nambu, "A New Field Effect Transistor with Selectively Doped GaAs/n-$Al_xGa_{1-x}As$ Heterojunctions," *Jpn. Appl. Phys.*, Vol. 19, 1980, pp. L225-L227.

[2] C.Z. Cil and S. Tansal, "A New Model for Modulation-Doped FET's ," *IEEE Electron Device Letters*, Vol. EDL-6, Aug. 1985, pp. 434-436.

[3] F.N. Trofimenkoff, "Field-Dependent Mobility Analysis of the Field-Effect Transistor," *Proc. IEEE*, Vol. 53, Nov. 1965, pp. 1765-1766.

[4] G.W. Wang ang W.H. Ku, "An Analytical and Computer- Aided Model of the AlGaAs/GaAs High Electron Mobility Transistor," *IEEE Transactions on Electron Devices*, Vol. ED-33, May 1986, pp. 657-663.

[5] D.L. Pulfrey and N.G. Tarr, *Introduction to Microelectronic Devices*, Prentice-Hall, Inc. 1989.

[6] K. Lee, M.S. Shur, T.J. Drummond, and H. Morkoc, "Current-Voltage and Capacitance-Voltage Characteristics of Modulation-Doped Field-Effect Transistors," *IEEE Transactions on Electron Devices*, Vol. ED-30, March 1983, pp. 207-212.

[7] S.C. Chapra and R.P. Canale, *Numerical Methods for Engineers*, McGraw-Hill, Inc. 1988.

[8] J.C. Sarker, *M.S. Thesis*, Electrical Engineering Department, University of Idaho, 1990.

[9] F. Ali and A. Gupta, *HEMTs and HBTs: Devices, Fabrications, and Circuits*, Artech House, Inc. 1991.